Characterization of Oscillations in Closed Drift Thrusters*

Edgar Y. Choueiri†
Electric Propulsion and Plasma Dynamics Laboratory
Princeton University, Princeton, NJ 08544, USA

Abstract

The nature of oscillations in the 1 kHz-60 MHz frequency range that have been observed during operation of closed drift thrusters (CDT), such as the stationary plasma thruster (SPT) and the anode layer thruster (ALT), is quantitatively discussed. We use contours of various plasma parameters measured inside the accelerating channel of an SPT[1, 2] as the starting point of our investigation and calculate the magnitude and spatial distribution of various associated natural and collision frequencies, characteristic lengths and velocities. This leads to a thorough characterization of the plasma in the channel under typical operation. This detailed picture is then used to evaluate the stability criteria and dispersion relations of oscillations that are suspected to occur. Using various dispersion relations, we present a band by band overview of the oscillations with a description of their observed behavior and discuss their nature and dependencies through comparison of the calculated contours to reported observations. In particular we discuss the excitation of low frequency azimuthal drift waves that can form a rotating spoke at lower values of B_r^*, axially propagating "transit-time" oscillations, high frequency azimuthal drift waves, ionization instability-type waves, and wave emission peculiar to weakly ionized inhomogeneous plasma in crossed electric and magnetic fields.

1 Introduction

1.1 Background

Closed drift thrusters (CDT) are Hall-type plasma accelerators that have been optimized in Russia during the past 25 years for high thrust efficiency ($\geq$ 50%). The original work on the CDT was conducted in the US in the early and mid-1960's[3] but interest in that accelerator was greatly diminished in favor of ion thrusters. Most of the work since, has been conducted in Russia. The name "closed drift" refers to the azimuthal drift of electrons that is common to all variants of such thrusters. The two main modern variants are the stationary plasma thruster (SPT) and the anode layer thruster (ALT)[1]. The former differs from the latter by its extended channel and the use of insulator chamber walls. Although the two have differentiating features in their operation and performance, they rely on the same basic principles for ionizing and accelerating the propellant. These principles were first correctly described and verified experimentally through the seminal work of Janes and Lowder (1965)[3]. These principles, and other features of modern CDT's, are also discussed in refs.[4, 5, 6, 7, 8]. A schematic of a CDT of the SPT type (i.e. extended channel) is shown in Fig. (1). Briefly, the underlying processes are as follows. The electrons from the cathode enter the chamber, and are subject to an azimuthal drift as a result of the crossed (mainly radial) magnetic and axial electric fields. The electrons in the closed drift undergo ionizing collisions with the neutrals (most typically xenon) injected through the anode. While the magnetic field is strong enough to lock the electrons in an azimuthal drift within the chamber it is not strong enough to affect the trajectory of the ions which are essentially accelerated by the axial electric field. A number of electrons equal to that of the produced ions reaches the anode due to cross-field mobility that often exceeds classical values, and the same number of electrons is thus available at the cathodes to neutralize the exhausted ions. Quasineutrality is therefore maintained and consequently no space-charge limitation is imposed on the acceleration resulting in relatively high thrust densities (especially compared to electrostatic ion propulsion). Nominal operating conditions with

*This work is supported by Space Systems Loral.
†Also, Theoretica, Applied Physics. Member AIAA.

[1]The stationary plasma thruster (SPT) is sometimes referred to as magnetic layer thruster, or thruster with extended acceleration zone, to differentiate it from the anode layer thruster (ALT), which is also operated in a stationary mode.

xenon are 2-5 mg/s mass flow rate, 200-300 V applied voltage and produce a plasma beam of about 170 eV (16 km/s) and a thrust of 40-80 mN at efficiencies of about 50%. Recently measured performance is reported in Refs. [9, 10].

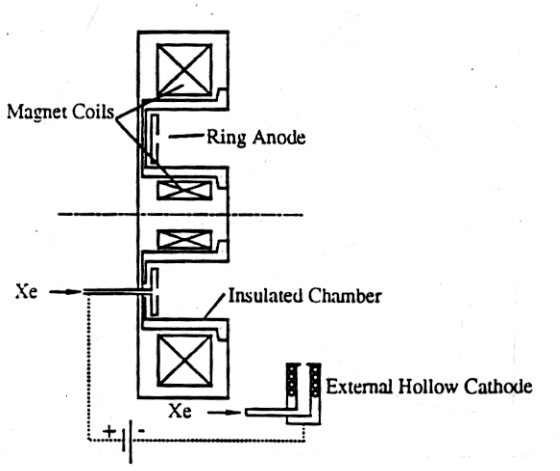

Figure 1: Schematic of a CDT with an extended channel (called SPT) showing the external cathode, the internal anode and the magnetic field coils. From ref. [11].

Due to their high specific impulse, their relatively high efficiency and high thrust density (they are not space-charge limited like ion thrusters) the CDT's are advantageous for near-term spacecraft propulsion applications and they have been selected by US industry and the government for development[12, 10, 9]. Since 1972, various types of CDT's were flown on Russian spacecraft most notably on more than 50 Meteor-series satellites, and they are routinely used in active space experiments[7].

1.2 Motivation

Because of the stringent requirements of US commercial spacecraft, which often require trouble-free thruster operation for more than 8000 hours, various efforts to improve aspects of the CDT performance are currently underway in Russia and the US. These include efforts to lower beam divergence[13], characterize electromagnetic interference[14], lower erosion rates[15] and lengthen lifetime. Strides towards even higher thrust efficiencies are also being made[16, 17]. Also, more compact power processing units (PPU) with specific masses around 5 kg/kW are sought to enhance the competetiveness of these thrusters[18]. Aside from low mass, a major requirement of the PPU is its ability to handle or suppress oscillations in the total circuit. The interaction between the PPU and its load can be quite complex due to the ubiquitous presence of oscillations. There is therefore an urgent need to characterize the nature and dependencies of these oscillations in order to aid the optimization of the PPU design.

Aside from its role in PPU design, the study of oscillations in the CDT could shed light on processes that play direct role in setting the performance level and efficiency of the device.

It should be stressed at the outset that oscillations in the CDT are not all necessarily adverse, and some are a natural part of the plasma processes that control transport, conduction and mobility in these devices. Since the earliest investigations[3], the role of oscillations in explaining basic features of the CDT, such as the enhanced electron diffusion to the anode, was recognized.

We also should clarify that the use of the word "instability" in the context of this paper does not refer to "unstable operation" of the thruster as whole but to the mechanisms that cause the oscillations[2].

1.3 Organization

In this paper we present a quantitative discussion of the nature of oscillations in the 1 kHz-60 MHz frequency range which could occur *inside* the SPT channel. We restrict our present study to oscillations of strictly plasma dynamical nature. In the next section we use contours of various plasma parameters measured inside the accelerating channel of the SPT as the starting point of our investigation and calculate the magnitude and spatial distribution of various associated natural and collision frequencies, characteristic lengths and velocities. This leads to a thorough characterization of the plasma in the channel under typical operation. This detailed picture is then used in the last section to evaluate the stability criteria of oscillations that are suspected to occur.

[2]The only exception is for the so-called "loop", "contour" or "circuit" oscillations which are discussed in Section 3.1 and which can cause the discharge to be extinguished . These low frequency oscillations, luckily, can be easily avoided as discussed in that section.

2 CDT Plasma Characterization

Before we proceed with the discussion of the various types of oscillations in the CDT, and in order to render that discussion quantitative, we conduct a thorough and spatially resolved characterization of the plasma inside the channel. For all our subsequent calculations, we use as initial input, the contour plots measured inside the channel by Bishaev and Kim[1]. Similar measurements were also reported by Bishaev et. al. in ref. [2]. These measurements were conducted in an SPT with a 10 cm diameter at a discharge voltage $U_d = 200$ V, a mass flow rate $\dot{m}$ =3 g/s of xenon and a discharge current of I_d = 3-3.2 A. The authors reported[2] that the dimensions of the probes used for these measurements were chosen to satisfy the requirements of the probe theories adopted for data reduction and that the measurement accuracy was checked using optical diagnostics. Other details concerning the experimental techniques can be found in these references.

2.1 Input Contours

First, the magnetic field, the radial variation of which may be neglected, was mapped axially with a Hall probe and is shown in Fig. (2).

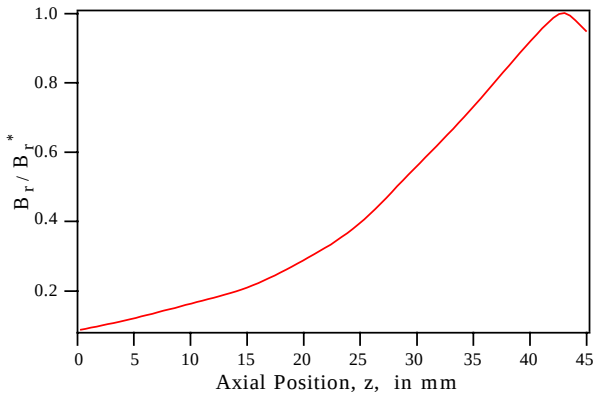

Figure 2: Axial profile of radial component of the magnetic field, B_r normalized by its maximum value B_r^* (with $B_r^* = 180$ G) as measured in ref. [1].

We digitized the contour data using a grid of 92 by 50 points with a spacing of .5 mm between points (corresponding to the resolution of the measurements). We then used the resulting matrices along with an image processing algorithm that we developed specifically for this task, to generate 8-bit color raster images showing the magnitude and spatial distribution of the measured parameters. An image enhancement algorithm was then used to smooth the contours for better visualization. Consequently, in all the color raster plots in this paper, the details of any structure whose dimension is smaller than .5 mm cannot be trusted as physical. The purple background surrounding each of the images correspond to regions where no experimental data were available. This is especially the case for many parameters near the walls. Also, the accuracy and reliability of the contours near the inlet or anode (specifically for axial locations $x \leq 15$ mm) are not good

Figures (8) to (12) show the resulting contours for electron temperature, charged species density, floating potential, charge density production rate and xenon neutral gas density consecutively. The inlet and anode are on the left side of the graphs, and the two parallel bottom and top grey lines represent the inner and outer insulator walls respectively.

The "hottest" region of the electron density map (Fig. (9)) is shown to be uniform at $6 \times 10^{17}\mathrm{m}^{-3}$. In reality, only the outer contour of the red region in that map was measured at that value. The lack of data inside that contour would artificially result in an infinite characteristic length for the density gradient in that region (i.e. uniform density). This is to be kept in mind later when looking at maps calculated using the density gradients.

2.2 Calculated Plasma Characteristics

The above mentioned measurements were used to calculate various parameters of interest. This created a thorough and spatially resolved characterization of the plasma. We calculated all the natural frequencies (ion and cyclotron frequencies ω_{ci}, ω_{ce}; ion and electron plasma frequencies ω_{pi}, ω_{pe}; the lower hybrid frequency, ω_{lh}) many collision frequencies (electron-neutral collision frequency ν_e; ion-neutral collision frequency ν_i, Coulomb collision frequencies; frequency of ionization by electron impact, etc.). All the characteristic length scales corresponding to these frequencies were also calculated. We also calculated all the associated particle velocities: the electron thermal velocity $v_{te} = (T_e/m_e)^{1/2}$; the Alfvén velocity; the ion velocity and the electron azimuthal and axial drift velocities).

In calculating the collision frequencies involving

electrons. we use for each grid point, experimentally measured cross-sections for xenon with the full energy dependence and calculate the convolution integrals using a Maxwellian velocity distribution for the electrons. For instance, for the total electron-neutral collision frequency, ν_e, we used:

$$\nu_e = n_a \int f(v) Q_e(v) v_{rel} dv \tag{1}$$

where v_{rel} is the relative velocity between the two species and Q_e is the total collision cross section obtained from experimental measurement[19] and shown in Fig. (3).

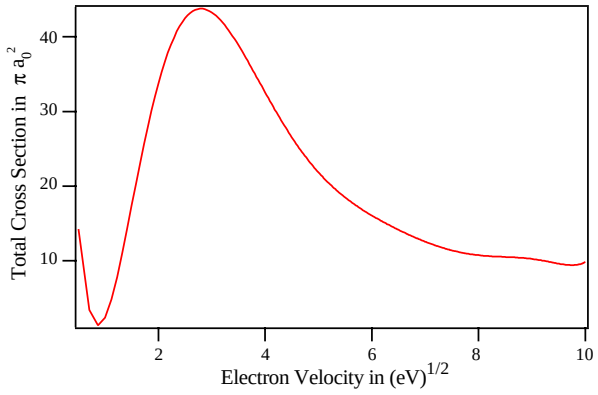

Figure 3: Total collision cross section for electrons in xenon from ref. [19]. a_0 is the Bohr radius.

When calculating the electron drift velocities we use the following equations:

$$u_{dex} = -D_{e\perp} \frac{\partial(n_e k T_e)}{n_e \partial x} - \mu_{e\perp} E_x \tag{2}$$

$$u_{dey} = \Omega_e u_{dex} \tag{3}$$

where

$$\mu_{e\perp} = \frac{\mu_e}{1+\Omega_e^2} \tag{4}$$

$$D_{e\perp} = \frac{D_e}{1+\Omega_e^2}, \tag{5}$$

are related to the electron mobility and diffusion coefficients

$$\mu_e = \frac{|e|}{m_e \nu_e} \tag{6}$$

$$D_e = \frac{k T_e}{m_e \nu_e}, \tag{7}$$

through the electron Hall parameter Ω_e:

$$\Omega_e = \frac{\omega_{ce}}{\nu_e}. \tag{8}$$

In Eqs. (2) and (3) we have treated each grid cell as imbeded in a rectangular coordinate system shown in Fig. (4), with the x-axis along the thruster axis (i.e. along the applied electric field E_x) and z-axis along the thruster radius (i.e. along radial magnetic field B_r). u_{dey}, therefore corresponds to the azimuthal electron drift velocity, which would be in the negative y direction. The application of this coordinate system to describe the entire channel carries the assumption of small channel curvature: $h/R \ll 1$, where h is the channel "height" and R its mean radius.

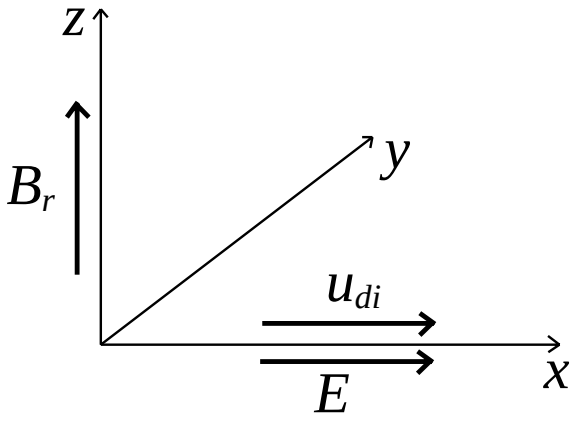

Figure 4: Rectangular coordinate system used in this paper. The x-axis is along the thruster axis (i.e. along the applied electric field E_x) and the z-axis is along the thruster radius (i.e. along radial magnetic field B_r). The y-axis, therefore corresponds to the azimuthal dimension.

All the above mentioned parameters were calculated for each point of the grid. In order to illustrate the ordering of the magnitudes of these parameters, the parameter from each spatial matrix was spatially averaged between the cross sections at axial positions x_1=2.5 cm and x_2=4 cm and plotted in Figs. (5) to (7). These three plots show the magnitude ordering of the relevant frequencies, characteristic lengths and velocities respectively[3]. In the

[3]The neutral gas temperature was assumed to be at the anode temperature of 1000 degrees K.

characteristic length plot of Fig. (6), we also show the calculated characteric lengths of the axial gradients of electron density, temperature and magnetic field, which will be important for our oscillation analysis[4]. The characteristic gradient length, $L_{\nabla\alpha}$, of a parameter α is given by:

$$L_{\nabla\alpha} \equiv \left| \frac{\alpha}{\partial\alpha/\partial x} \right| = \left| \frac{\partial \ln \alpha}{\partial x} \right| \tag{9}$$

where x is the axial dimension.

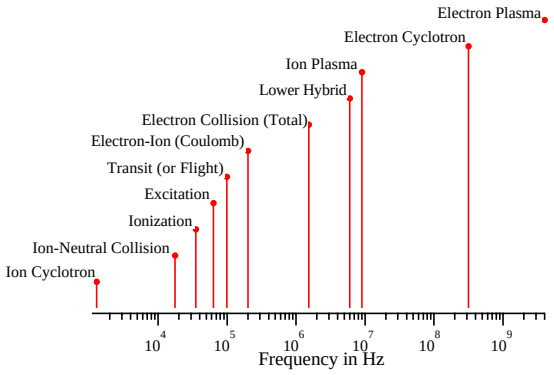

Figure 5: Magnitude ordering of relevant frequencies. (Spatially averaged between the cross sections at axial positions x_1=2.5 cm and x_2=4 cm).

For further illustration, we chose the spatial maps of the following parameters: electron-neutral total collision frequency ν_e, ionization frequency ν_{ioniz}, the axial electric field E_x (obtained by calculating the gradient of the applied potential), the ion velocity u_i, the electron azimuthal drift velocity u_{dey} and the electron Hall parameter Ω_e. These are shown in Figs. (13) to (18) consecutively.

The total electron-neutral collision frequency ν_e, shown in Fig. (13) was calculated using Eq. (1) and its spatial distribution, to a large extent, reflects the neutral xenon distribution in the channel shown in Fig. (12). This frequency, as we shall see later in Section 3.3.2, sets an upper limit for one type of oscillations. Its average between x_1=2.5 cm and x_2=4 cm is 1.53 MHz. The xenon ionization frequency ν_{ioniz} by electron impact, shown in Fig. (14), is also important since it represents the characteristic oscillation of the ionization instability discussed

[4]In calculating the characteristic length of the electron density gradient we neglected the weight of the central region (red spot in Fig. (9)) which, as mentioned earlier, would have yielded very large lengths.

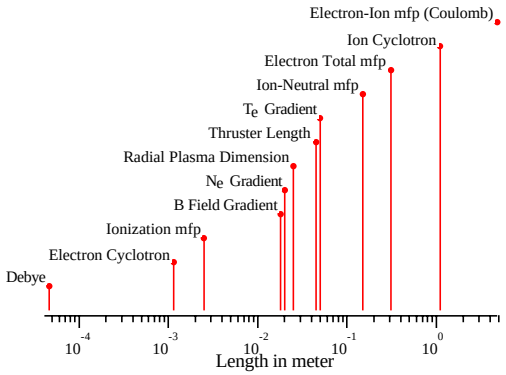

Figure 6: Magnitude ordering of relevant lengths. (Spatially averaged between the cross sections at axial positions x_1=2.5 cm and x_2=4 cm).

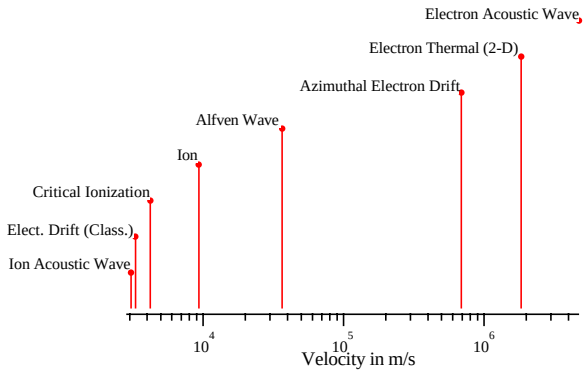

Figure 7: Magnitude ordering of relevant velocities. (Spatially averaged between the cross sections at axial positions x_1=2.5 cm and x_2=4 cm).

later in Section 3.3.2. The axial electric field shown in Fig. (15) shows regions with values as high as 20 kV/m, which explains the electron heating seen in the same regions in the measured electron temperature plot of Fig. (8). The ion velocity map of Fig. (16) shows that the ions can reach velocities as high as 14 km/s. It is interesting to note from that plot that the highest velocities are attained near the downstream end of the inner insulator wall. This fact combined with the flow direction measurements in that region shown in ref. [1], hint to the role played by ion sputtering in insulator erosion. The electron drift velocity in the azimuthal direction u_{dey}, calculated with Eq. (3) is shown in Fig. (17). Its average between x_1=2.5 cm and x_2=4 cm is 690 km/s. Again,

the regions of substantial acceleration in that map corresponds to those of high electric field in Fig. (15). Finally, the electron Hall parameter Ω_e is shown in Fig. (18). It is much larger than unity over the entire grid and averages about 286 between x_1=2.5 cm and x_2=4 cm. The corresponding average for the ion Hall parameter Ω_i (not shown here) is .15. This is characteristic of the CDT whose design obeys the inequalities: $\Omega_i < 1 \ll \Omega_i$. This high value of the Hall parameter implies, through Eq. (3), that the cross-field drift velocity towards the anode is, on the average, about 300 times smaller than the azimuthal drift velocity. This estimate is based on a classical treatment of cross-field mobility and diffusion. The real value of the axial electron current can be calculated by subtracting the measured ion current from the discharge current and is often much higher than the classical value given by Eq. (2). Quite often, as we shall see below, one must invoke the role of plasma oscillations to explain the actual cross-field mobility and diffusion of the electrons when the magnetic field is high.

With the above characterization, we have a detailed and experimentall-based picture of the plasma in the CDT, with which we can proceed to a quantitative study of the oscillations.

3 Overview of Observed Oscillations

The CDT plasma has a very rich and complex wave and noise characteristics over a wide frequency spectrum. The character of these oscillations range from narrowband and very coherent waves with well defined propagation angles, to broadband turbulence. Many of the oscillations are inherent to the ionization, particle diffusion and acceleration processes of the device and can be considered as "natural" modes excited by the plasma to "self-regulate" the charged particle production and diffusion processes in order to adjust to a particular imposed operating mode.

Oscillations over a wide spectrum of frequencies have always been observed in the terminal characteristics of Hall-type thrusters. During the 1970's several experimental studies dedicated to the observation of oscillations and the measurements of their characteristics were conducted in Russia[8, 20, 21, 22].

The amplitude and frequencies of observed oscillations were found to be strongly dependent on operating conditions: mass flow rate, applied voltage, initial and time-evolving geometry, degree of contamination of the discharge chamber, cathode characteristics (mass flow rate and location), PPU characteristics and configuration and most strongly the magnetic field profile and magnitude. Furthermore, when spatially resolved probing of the oscillations was conducted[22] inside the channel it was revealed that the oscillation spectra also depend on the axial location inside the channel.

This multi-parameter dependence renders the oscillation picture too complex for straightforward description. However, the strong dependence on the magnetic field offers the opportunity to describe the oscillation spectra as a function of the maximum value of the magnetic field B_r^* (usually reached a few millimeters upstream of the exit) with all other operating parameters (geometry, mass flow rate, discharge voltage) held constant[5]. This was attempted by Tilinin[22] who conducted extensive measurements of the spectra in the range 10 kHz-400 MHz at four axial locations in the channel, and under a wide range of operating conditions. He identified six major regimes of operation, depending on the range of B_r^*, with each regime characterized by a general spectrum of oscillations and a range for the discharge current.

A review of these measurements and others[8, 20, 21] is summarized in Table 1. We discussed below these observations band by band.

Due to the urgency of optimizing the design of the power processing unit (PPU) for flight-ready modules, frequencies higher than a few tens of MHz are not considered in detail in the present study since only lower frequency oscillations seem to impact the PPU design.

3.1 Oscillations in the Frequency Band 1-20 kHz

3.1.1 Observed Behavior

Oscillations in this frequency band are often referred to in the Russian literature as "loop"[22], "circuit"[23] or "contour"[23, 24] oscillations. When B_r^* is increased to about half its optimal value (Regime IIIa in Table 1) these oscillations become prominent and their amplitude can reach 10% of the total voltage amplitude. For $B_r^*/(B_r^*)_{\rm opt}$ between .8 and 1, these oscillations are relatively damped. This regime of operation is called "optimal"[22] (Regime IV in Table 1). The oscillations become violent as

[5]This leaves the discharge current to be a unique function of the magnetic field.

Regime	I	II	IIIa	IIIb	IV	V	VI
$B_r^*/(B_r^*)_{\rm opt}$	$< .38$	.38-.47	.47- .6	.6- .76	.76- 1	1- 1.35	$1.35 \leq$
1-20 kHz	1	1	8	8	3	10	4
20-60 kHz (Azimuthal waves)	0	6	0	4	2	0	0
20-100 kHz	1	5	4	6	7	6	4
70-500 kHz	1	4	4	7	7	6	8
2-5 MHz (Azimuthal waves)	1	3	3	4	5	1	1
.5-10 MHz	1	3	3	4	5	5	6
10-400 MHz	1	3	2	3	4	5	5
>GHz	NA	NA	NA	NA	NA	NA	NA

Table 1: Character of measured oscillation spectra as a function of the maximum value of the magnetic field B_r^* normalized by its optimal value ($(B_r^*)_{\rm opt} \simeq 170$ G for $\dot{m} = 4$ mg/s, $U_d = 200$ V and an SPT with a diameter of 9 cm operating with xenon). The numbers represent the relative importance of a given frequency band to the overall spectrum. The scale is 1 to 10 where 1 is weak amplitude (below the sensitivity of the diagnostics) and 10 is dominant amplitude of the same order as the applied voltage. 0 means that the oscillations in that band were absent and NA denotes unavailable data. The digits are relative within a given band of frequencies and not across the bands. Based on experimental data and oscillograms from refs. [8, 20, 21] and especially ref. [22].

soon as B_r^* is increased a little above its optimal value (Regime V in Table 1). Their amplitude can reach as high as 100% of that of the DC voltage, often causing the discharge to be extinguished. Since at $B_r^* = (B_r^*)_{\rm opt}$ the ratio of the ion current at the exit to the discharge current reaches a maximum and any further increase in B_r^* causes a severe onset of oscillations in this frequency band, the CDT is typically operated just below that onset in the so-called "optimal regime" (Regime IV in Table 1).

3.1.2 Physical Description

By operating in the"optimal" regime (Regime IV in Table 1) which, for a fixed thruster, mass flow rate $\dot{m}$ and discharge voltage V_d can be reached by changing B_r^*, the violent oscillations in this band can be avoided. Moreover, these oscillations are known to be quite sensitive to the entire circuitry including the PPU (hence their name "circuit" or "loop" oscillations). The use of the proper matching filter in the circuit can be instrumental in further reducing their amplitude. This in fact was done for all but the newest generation of thrusters. A commercial-grade SPT-100 PPU is currently being optimized and it is now known that the parameters of the external circuit significantly influence the oscillation characteristics in the broader frequency range[23].

Since the violent manifestation of these oscillations can be largely avoided by operating in the optimal regime, they have not received in-depth analysis in the literature comparable to the extent to which other oscillations and instabilities were studied. The exact mechanism(s) behind their onset is not clear and sometimes, in the Russian literature, it is related to the "instability of the position of the zone of ionization"[4].

3.2 Oscillations in the Frequency Band 20-60 kHz with Azimuthal Propagation

3.2.1 Observed Behavior

In this frequency band, oscillations with azimuthal propagation must be differentiated from other oscillations with comparable frequencies but that do not propagate azimuthally. The first reported observation of these azimuthal waves was made by Janes and Lowder[3]. More detailed experimental studies of

these waves, using cross-correlation techniques, were conducted in refs. [8, 20, 21]. Typical oscillations in this band were observed with a phase velocity of the same order as the E/B drift velocity propagating azimuthally. The associated waves form a rotating spoke. These oscillations typically appear at their strongest when B_r^* is a factor of about .38 to .47 times the optimal field (i.e. Regime II in Table 1) reaching peak amplitudes of about 10% that of the DC voltage. The fundamental oscillation appears with up to 8 harmonics but they are abruptly damped if the magnetic field is slightly increased (Regime IIIa). A further increase in B_r^* would cause these azimuthal oscillations to reappear but they are not a prominent part of the spectrum. Operation in the optimal regime leads to a substantial reduction in their amplitude, which then decreases with increasing B_r^*.

For a fixed magnetic field (profile and magnitude), the appearance and amplitude of these azimuthal oscillations depend on the location of the operating point along the current-voltage curve of the thruster[20]. They are dominant at low discharge voltage, tend to diminish at higher voltage, and become very weak in the current saturation part of the current-voltage characteristic, except in the vicinity of the anode.

Finally, it is worth mentioning that an investigation of the behavior of these azimuthal waves as a function of the magnetic field profile[8] showed that their amplitude increases by as much as a factor of 5 to 8 if the axial gradient of the magnetic field is reversed from positive (B_r increasing with distance from the anode) to negative (keeping the power constant).

3.2.2 Physical Description

The nature of these azimuthal waves and and the mechanisms behind their generation, have been the subject of several experimental and theoretical studies, and in consequence are now relatively quite well understood[3, 8, 20, 21].

The earliest experimental study[3] using azimutahlly positioned probes, already demonstrated that the waves form a rotating spoke with a phase velocity[6] about $.2 \times E_x/B_r$. The spoke, which has one end near the anode, is also tilted azimuthally by about 15 to 25 degrees. Janes and Lowder[3] showed that this azimuthally rotating spoke plays a major role in enhancing electron transport to the anode.

[6]In ref. [8] a factor of .4 to .8 was measured.

This anomalous transport or diffusion can be explained on the basis of a cross-field drift due to the crossing of B_r and E_θ, where the latter is the azimuthal oscillating electric field associated with the potential oscillations. Indeed, measurements show that the electron currents produced by this drift agrees with the experimentally inferred axial electron current. Although they were able to explain the role these oscillations play in anomalous electron diffusion, Janes and Lowder only *speculated* on the underlying origin and mechanisms as probably related to an "ionization wave". It seems that this early speculation, may have caused the association of the word "ionization" with the rotating spoke.

Although these oscillations are often haphazardly related to an "ionization instability", in the Russian literature, the models developed to explain them do not explicitly involve the ionization kinetics. Indeed one of the earliest theories[8] that modeled their stability criteria, frequencies and growth rates, was based on a simple non-reacting (i.e. no ionization or recombination) two-fluid ideal MHD formulation ($\Omega_e = \infty$) without an energy equation. By linearizing the corresponding equations for small amplitude planar waves, Morozov et al.[8], find a simple dispersion relation which can yield unstable modes depending on the sign and magnitude of the ion drift velocity u_{di}, the electron azimuthal drift velocity u_{de} and the following relative inhomogeneity scale parameter

$$\frac{B_r}{n_e}\frac{\partial}{\partial x}\left(\frac{n_e}{B_r}\right). \tag{10}$$

For typical CDT parameters, with $u_{dey} < 0$ and $u_{di} > 0$, they find that an instability in the frequency band in question can exist for cases where $\partial B_r/\partial x < 0$.

In order to carry a quantitative study of these azimuthal oscillations for our case, we choose to apply the more general dispersion relation derived by Esipchuck and Tilinin[21] who also show that the dispersion relation of Morozov et al.[8], is but a special case of their more general description.

Again, the starting equations are those of a two-fluid MHD *collisionless* plasma description which, after the following assumptions: 1) unmagnetized ions (i.e. $r_{ci} \gg L$ where r_{ci} is the ion cyclotron radius and L is the device length), 2) relatively weak inhomogeneity

$$L < L_{\nabla B_r}, L_{\nabla n_e}, \tag{11}$$

and for the frequency range, $\omega_{ci} \ll \omega \ll \omega_{ce}, \omega_{pe}$ (where ω is the frequency of the oscillations in question), can be linearized using oscillatory disturbances

of the form

$$\alpha = \alpha_0 + \tilde{\alpha} \exp\left(k_x x + k_y y - i\omega t\right) \tag{12}$$

where α is any of the variables of the problem, α_0 its steady-state value, and $\tilde{\alpha}$ is the amplitude of its oscillatory component. Linearization means an assumption of small amplitude, i.e. $\tilde{\alpha} \ll \alpha_0$. This will yield the following dispersion relation[8]

$$1 - \frac{\omega_{pi}^2}{\left(\omega - k_x u_{di}\right)^2} + \frac{\omega_{pi}^2}{\omega_{ci}\omega_{ce}} + \frac{\omega_{pi}^2}{k^2 v_A^2} - \frac{\omega_{pi}^2 k_y \left(u_{dey} - u_B\right)}{k^2 u_{di}^2 \left(\omega - k_y u_{dey}\right)} = 0. \tag{13}$$

where v_A is the Alfvén velocity $v_A = B^2/\mu_0 M_i n_i$, M_i is the ion mass, k is the wavenumber $k = 2\pi/\lambda$, (λ is the wavelength of the oscillations), k_x and k_y are the components of the wavevector $\boldsymbol{k}$ along the applied electric field and the azimuthal direction respectively (see Fig. (4)). An important parameter in the above equation is the magnetic drift velocity u_B,

$$u_B \equiv \frac{u_{di}^2}{\omega_{ci} L_{\nabla B}} \tag{14}$$

where, again, $L_{\nabla B}$ is the characteristic length of magnetic field gradient as defined in Eq. (9). In order to study the stability of low frequency electrostatic waves, Esipchuck and Tilinin[21] considered the case of the frequencies bounded by

$$\left(\omega - k_x u_{di}\right)^2 \ll \frac{k^2 v_A^2 \omega_{ce}\omega_{ci}}{k^2 v_A^2 + \omega_{ce}\omega_{ci}} \tag{15}$$

and furthermore added one more assumption 3)

$$\omega_{lh} \simeq \left(\omega_{ci}\omega_{ce}\right)^{1/2} \ll \omega_{pi} \tag{16}$$

where $\omega_{lh} \simeq \left(\omega_{ci}\omega_{ce}\right)^{1/2}$ is the lower hybrid frequency. Under all these assumptions the dispersion relation Eq. (14) has the following roots:

$$\omega = k_x u_{di} - \frac{k^2 u_{di}^2}{2k_y \left(u_{dey} - u_B\right)} \pm \frac{k u_{di}^2}{2\left(u_{dey} - u_B\right)} \times \left[\left(\frac{k_x}{k_y}\right)^2 - 4\frac{k_x \left(u_{dey} - u_B\right)}{k_y u_{di}}\right. \tag{17}$$

$$\left. + 4\frac{u_{dey}\left(u_{dey} - u_B\right)}{u_{di}^2} + 1\right]^{1/2} \tag{18}$$

Before we apply the above equation to our particular numerical study, we ought to discuss briefly Esipchuck and Tilinin's assumptions as listed above. First, assumption 2), namely that of weak homogeneity, is not amply satisfied over the channel and, as it can be seen from Fig. (6), on the average, the gradient lengths are all smaller than the device length. They are however of the same order of magnitude. Second, assumption 3), namely that the ion plasma frequency be much larger than the lower hybrid frequency, is also, on the average, not strongly the case for the typical SPT case considered here as can be seen from Fig. (5). Bearing this in mind, we proceed with a stability evaluation using Eq. (18) which, as we shall see, does predict the main features of the experimental observations.

For our particular study case, we calculated the roots in Eq. (18) which are of the form

$$\omega = \omega_r + i\gamma \tag{19}$$

(where ω_r is the frequency, and γ, the imaginary part, is the growth rate. We selected the grid points where the above equation yields roots with positive imaginary solutions (i.e. $\gamma > 0$) which, from Eq. (12) correspond to growing oscillations, i.e. instability.

The frequencies of unstable waves were calculated according to Eq. (18) for the first mode i.e. $k = 2\pi/\lambda = 1/r$ where r is the radius of a given grid point. Furthermore, since we are looking for azimuthal modes we chose a largely azimuthal propagation with $k_y = 10\ k_x$. The resulting map is shown in Fig. (19) where the color purple denotes stability. It can be readily seen that the plasma is stable to these disturbances for most of the channel except for a small region which clearly falls in the part of the plasma where $\partial B_r/\partial x < 0$, as can be noted by looking at the magnetic field profile in Fig. (2). The existence of an instability in regions of negative axial gradient of B_r, is in agreement with the experimental observations mentioned above as reported in ref. [8]. Indeed, the choice of a B_r profile with $\partial B_r/\partial x > 0$, such as the one applied to the device that produced the data used here, was motivated by stability considerations resulting from studies with various B_r profiles such as that of ref. [8].

Furthermore, the fact that the instability region shown in Fig. (19)is very limited in extent is in agreement with the observation, reported above, that the low frequency azimuthal waves are greatly diminished during operation with B_r^* at or above $(B_r^*)_{\text{opt}}$ (Regime IV and above in Fig. (1)). Indeed, we should keep in mind that the experimental data used for our calculations were obtained while the thruster was operated in the "optimal" regime (Regime IV in Fig. (1)). The range of excited frequencies as calcu-

lated and shown in that map, is 25 to 55 kHz which is in agreement with the measured frequencies of these azimuthal waves.

Further agreement with experiments can be noted by calculating the phase velocity, v_ϕ, of the unstable waves $v_\phi = \omega/k = f\lambda$. This is shown in the map of Fig. (20) where the phase velocity is normalized by the azimuthal electron drift u_{dey} (shown in Fig. (17)) which is very close to E_x/B_r (because of $\Omega_e \gg 1$. The phase velocities are in the range .1 to .2 E/B, in agreement with values measured in the above mentioned experimental studies.

Finally, the experimental observation, also reported above, that azimuthal waves in this frequency, for operation on the current saturation part of the current-voltage characteristic, are favored to exist close to the anode, cannot be checked by our calculations due to the poor state of the experimental contour data we have for that region[7].

Conclusions regarding the nature of oscillations in this band: Oscillations with azimuthal propagation in this band seem to be low frequency electrostatic waves with strongly azimuthal propagation ($k_x \ll k_y$). These waves have been shown to play an important role in insuring suitable electron diffusion towards the anode when Coulomb collisions do not suffice. They are rendered unstable (i.e. excited) by the presence of gradients of magnetic field and density. These gradients can have the signs and magnitudes to present a free energy source for electrostatic perturbations to grow. The free energy source can be related to a drift velocity associated with the gradient (such as in Eq. (14)) and the instability can therefore be called a "drift" instability in accordance with widespread plasma physics nomenclature. Furthermore, since the general dispersion relation in Eq. (14), with u_B and u_{dey} both set to zero, is often associated with fast magnetosonic waves, Esipchuck and Tilinin[21] propose the name "drift magnetosonic waves".

From, an engineering point of view, these waves do not in principle represent a formidable problem to CDT operation since the thruster is nominally operated in the optimal regime. However, the "reappearence" of these modes due to changes in local conditions brought about by changes in geometry over the life of a particular device, is in principle possible, and remains to be investigated. As regards to this point, there seems to be a lack of rigorous experimental data correlating the appearance of these waves as a function of operation time.

[7]The relatively benign manifestation of these waves during operation in the "optimal" regime does not warrant a detailed study of the dispersion relation to determine the wavenumbers and propagation angles that condition the most dominant modes i.e. the roots with the largest growth rate.

3.3 Oscillations in the Frequency Band 20-100 kHz

3.3.1 Observed Behavior

Aside from the azimuthal waves whose frequencies fall in within this range, there seems to be another types of oscillation that can contribute to this band of the spectrum. Even in the absence of the low frequency azimuthal waves described above, the measured spectra show considerable energy in that range (*cf* Table 1). This is the case even for operation in the "optimal" regime. Since the well defined azimuthal waves, described above, fall within that band, other possible contribution from non-azimuthal oscillations did not receive as much characterization in the literature.

3.3.2 Physical Description

From Fig. (5), it can be seen that this band falls between the ion collision frequency and the electron collision frequency. Also, from the same figure, we can see that the characteristic frequency for the incoming xenon neutrals by electron impact falls also in that range. It is therefore natural to suspect that mechanisms related to collisions with neutrals (which dominate in weakly ionized plasmas) and/or ionization are playing roles in this band. We shall look, albeit briefly, at each of these two possibilities.

Instabilities Related to an Inhomogeneous and Weakly Ionized Plasma. The ionization fraction calculated from Figs. (9) and (12) and averaged over all grid points between x_1=2.5 cm and x_2=4 cm is .028. For xenon, the cross sections are such that, at these electron temperatures (average T_e is about 13 eV from Fig. (8)), collisions with neutrals dominate. The dispersion relation in Eq. (14) was derived from a collisionless description and although it is capable of describing the azimuthal oscillations in a slightly lower frequency band (and as we shall see in Section 3.6, in a higher band), it does not lead to unstable modes in this band other than for azimuthal propagation. Adding the effects of collisions to the governing equations that yielded Eq. (14),

would greatly complicate the derivation of the dispersion relation. For the sake of simplicity, and to illustrate the possible instabilities of an inhomogeneous weakly ionized plasma, we shall make one major assumption, namely the neglect of the applied DC electric field. Under this assumption there exist several classical treatments of the problem[25, 26, 27].

In ref. [27] the relevant case of oscillations in the frequency range

$$\nu_i < \omega < \nu_e \tag{20}$$

is treated. It is shown that oscillations with frequencies and growth rates given by

$$\omega_r \simeq \gamma \simeq k \left(\frac{T_e}{M_i} \right)^{1/2} \tag{21}$$

(where one recognizes the ion acoustic velocity $u_{ia} = (T_e/M_i)^{1/2}$) can become unstable if the following inequality regarding the strength of the density gradient holds

$$L_{\nabla n_e} \leq \frac{T_e}{\omega_{ce} m_e} \left(\frac{M_i}{T_e} \right)^{1/2} \tag{22}$$

which is equivalent to stating that the inhomogeneity must be strong enough so that $L_{\nabla n_e}$ is smaller than a characteristic cyclotron radius r_{ca} based on the ion acoustic velocity and the ion cyclotron frequency ($r_{ca} \equiv u_{ia}/\omega_{ci}$). This, along with Eqs. (20) and (21), gives oscillations bounded by

$$\nu_i < \omega_r \leq \omega_{\nabla n_e} < \nu_e \tag{23}$$

where $\omega_{\nabla n_e}$ is the electron drift frequency

$$\omega_{\nabla n_e} \equiv \frac{T_e k}{m_e \omega_{ce} L_{\nabla n_e}} \tag{24}$$

Figure (21) shows the minimum bound on the frequencies of oscillations whose wavelengths are contained inside the SPT. Only grid points satisfying the criterion in Eq. (22) are shown. The rest (purple color) correspond to stable conditions. It is clear that oscillations in the band in question can be produced. In Fig. (22), the corresponding wavelengths are shown.

Instabilities related to Ionization. All of the instability mechanisms we have considered so far, do not (at least explicitly) take into account the ionization process as a potential source of instability. The *ionization instability* in a weakly ionized gas is described by Smirnov[28] as follows. Due to ionization, the electron density may increase in a certain region. Due to the presence of currents through that region, the evolution and absorption of energy are altered. If the energy increase is higher than the energy transferred from the electrons through collisions with the neutrals, the electron density may grow further because of its dependence on the temperature, leading to an unstable process.

Smirnov[28], treats the case of the ionization instability of a weakly ionized plasma in a crossed electric and magnetic fields. By setting up a balance equation for the electron energy per unit volume, taking into account the energy transferred from electrons to the neutrals through elastic collisions, and the relationship between perturbations of the temperature and density, the following rqte equation is found

$$\frac{d}{dt} \left(\frac{3}{2} n_e T_e \right) = \tilde{n_e} m_e u_{de}^2 \nu_e \left[\frac{\left(\omega_{ce}^2 + \nu_e^2 \right)^{1/2}}{\nu_e} - 1 - \frac{T_e}{\epsilon_i} \right] \tag{25}$$

where ϵ_i is the first ionization potential of the neutrals. This yields the following instability criterion

$$\left(\frac{2T_e}{\epsilon_i} \right)^{1/2} \leq \Omega_e \tag{26}$$

Although the case seems quite similar to the CDT, there are two major differences. First there was a simplifying assumption that ν_e is largely independent of T_e. Second, in that derivation, there was an allowance for a y-component of the electric field of the order $\Omega_e E_x$ which would force the electron current to flow almost axially. Keeping these differences in mind, we have evaluated the criterion in Eq. (26) in the form $\Omega_e / \left(2T_e/\epsilon_e \right)^{1/2} \geq 1$, over the entire grid. The map in Fig. (23) shows the regions of instability and the extent to which the criterion is satisfied. Most likely, the quantitative relevance of this map to our problem is not good in view of the two differences listed above, but if the picture is to be trusted qualitatively, it would be interesting to note the region where the criterion is most satisfied. This region, being near the exit of the inner insulator is the region that is most subjected to geometrical changes, due to erosion or deposition of sputtered material[8]. There is therefore a tentative link between the appearance of these oscillations and the operation-time dependent geometry.

The time scales associated with this kind of instability are of the same order as the ionization time

[8]There are indications that the rate of erosion decreases with operation time and that deposition of sputtered material may be more responsible for geometry change than erosion[29]

scales. Therefore we can refer to Fig. (14) for the relevant frequencies which fall within the frequency band being considered here[9].

Conclusions regarding the nature of oscillations in this band: The oscillations in this band seem to be related to either a gradient-driven instability that is peculiar to weakly ionized plasma or an ionization-type instability. It is also possible tat both mechanisms contribute to the spectrum in this band.

3.4 Oscillations in the Frequency Band 70-500 kHz

3.4.1 Observed Behavior

Oscillations in this frequency band are often called "transient-time" oscillations in the Russian literature[20] because they have frequencies that roughly correspond to u_{di}/L. These waves were first measured and characterized experimentally by Esipchuck et. al.[20] and their experimentally observed characteristics are well documented in that paper. Here we list briefly some of their major features. They are quite active during operation at the "optimal" regime. With all parameters fixed and B_r increasing, these oscillations first become prominent as Regime IIIb is reached with their amplitude reaching several volts (cf. Table 1). They increase in importance with increasing B_r^* and their amplitude can become as high as 30% of the discharge voltage. Their amplitude distribution over the channel strongly depends on the profile of B_r. Their overall spectrum seems to be quite independent of $\dot{m}$ at fixed U_d. They are largely turbulent but still preserve some deterministic space-time correlations. They are believed to be essential for turbulence-driven or anomalous diffusion which becomes necessary at higher B_r due to the inadequacy of classical mobility and diffusion.

3.4.2 Physical Description

The name "transient-time" oscillation is quite appropriate since a frequency ω_r of

$$\omega_r \simeq k_x u_{di} \frac{b}{b+1} \tag{27}$$

where $b \equiv u_B/|u_{dey}|$, can be obtained from the dispersion relation in Eq. (14) for the following conditions[21]

$$k_y^2 \ll k_x^2 \tag{28}$$

which implies an almost axially propagating wave[10] and the inequality

$$u_B > \frac{1}{2}\left[\left(u_{dey}^2 + u_{di}^2\right)^{1/2} - |u_{dey}|\right]. \tag{29}$$

In Fig. (24) we show the calculated frequencies in regions of instability. The excited waves, have frequencies between 60 and 800 kHz for our case study. It can be directly noted that the region with negative B_r gradient is stable which is in agreement with observations. Furthermore, the highest frequencies are confined just to the left of B_r^*. This is also the case for the growth rate which is given by[21]

$$\gamma \simeq k_x u_{di} \frac{\sqrt{b}}{b+1}. \tag{30}$$

and therefore scale similarly to the frequencies. This confinement is in good agreement with what was observed with spatially resolved probing[20, 22]. Finally, the "quenching" of these oscillations with diminishing B_r reported in the experimental literature is also apparent from Fig. (24) where the frequencies (and hence the wavelengths) diminish with decreasing B_r to the left of the maximum value.

Conclusions regarding the nature of oscillations in this band: These oscillations are quasi-axial electrostatic waves with a relatively broad and mixed band. They tend to be relatively turbulent and are presumed to play an important role in regulating the plasma transport. Their characteristics and dependencies are well predicted by the linear theory of gradient driven magnetosonic waves with almost axial propagation ($k_y \ll k_x$). Physically they are due to the coupling of the "beam mode" $k_x u_{di}$ to the oscillations driven by the inhomogeneity. Due to their strong scaling with ku_{di}, they are often called "transient-time" oscillations.

[9] Within the context of ionization-type instabilities, we should mention the work of Kim[23], which unfortunately has not yet been published in English. That analysis relies on estimating the time delay associated with the transit of various species from one region of the discharge to the other and yields values for the frequencies that fall within observed frequency bands.

[10] We avoid here using the word "longitudinal" or "quasi-longitudinal" common in the English translation of Russian plasma physics papers. We prefer to use the words "axial" or "quasi-axial" since the word "longitudinal" in the English plasma physics literature refers to the electrostatic nature of the waves (i.e. the k vector is along the oscillating electric field) and not to their propagation direction.

3.5 Oscillations in the frequency band .5-5 MHz and Higher

3.6 Observed Behavior

Like the "transient-time" oscillations discussed above, oscillations at higher frequencies become more prominent as B_r^* is increased, as illustrated in Table 1. Even for operation at the optimal regime, oscillations and "noise" with frequencies near and higher than those of the "transient-time" oscillations are more important than the lower frequencies such as the "circuit" and low frequency azimuthal waves which become very weak.

It is interesting to note that one mode of high frequency oscillation seems to have been discovered theoretically by Esipchuck and Tilinin[21] before it was observed experimentally. The same authors looked for the theoretically predicted mode using probes and high frequency instrumentation and found it to exist. This mode has the following observed behavior. The propagation is mostly azimuthal like the low frequency azimuthal drift wave described in Section 3.2. The fundamental frequency is (for optimal operation with xenon and nominal conditions) in the 2 to 5 MHz range. In that frequency range, it is possible to see this mode by using azimutahlly spaced probes and most often the first azimuthal mode is observed (i.e. $k = 1/R$) and sometimes the second azimuthal mode is detectable. The phase velocity is close to u_{dey} and is in the negative y-direction. A reversal of the direction of the field would reverse the direction of propagation. While the amplitude is raised with increasing B_r^*, the fundamental frequency drops.

Aside from this azimuthal mode, the high frequency oscillations in the CDT seem to be have received less attention than their lower frequency counterparts.

3.6.1 Physical Description

The theoretically predicted high frequency mode was arrived at also through the dispersion relation of Eq. (14) after more simplifying assumptions. The fact that the same equation, which as we discussed above, had some border-line assumptions, could describe observed modes at three widely different frequency ranges: lower frequency azimuthal waves, quasi-axial "transient-time" oscillations and this high frequency azimuthal mode (all contained within the wide range $\omega_{ci} \ll |\omega| \ll \omega_{ce}$) is a testimony to its usefulness and overall validity.

Instead of looking at these higher frequencies with that dispersion relation –an effort already accomplished analytically by Esipchuck and Tilinin[21]– we opt to use another formalism that emphasizes the collisional nature of the plasma. This is one facet, the collisionless treatment of refs. [21, 30] are missing.

The case of a weakly ionized plasma in a crossed electric and magnetic field has been treated in a classic paper by Simon[31]. The formulation developed in that paper extends the simpler description of an inhomogeneous weakly ionized plasma (that we used in Section 3.3.2 to study the lower frequency waves) to include the effect of an applied electric field. The field can be shown to be destabilizing for higher frequencies[27]. We follow Simon's assumption[31] that the plasma is finite only in the x direction. This would not greatly affect our wave analysis since we will be looking only at "flute modes" i.e. $k_z = 0$ and $k = \pm k_y$ which for our geometry correspond to azimuthal modes. By assuming that the most relevant gradient is that of the charged particle density, we quote the momentum equations for the ion and electron fluxes, Γ

$$\begin{aligned}
\Gamma_x^\pm &= \left(-D_\perp^\pm \frac{\partial n}{\partial x} \pm \mu_\perp^\pm n E_x\right) \\
&\quad \mp \Omega_\pm \left(-D_\perp^\pm \frac{\partial n}{\partial z} \pm \mu_\perp^\pm n E_z\right) \\
\Gamma_y^\pm &= -D_\parallel^\pm \frac{\partial n}{\partial y} \pm \mu_\parallel^\pm n E_y \qquad (31) \\
\Gamma_z^\pm &= \left(-D_\perp^\pm \frac{\partial n}{\partial z} \pm \mu_\perp^\pm n E_z\right) \\
&\quad \pm \Omega_\pm \left(-D_\perp^\pm \frac{\partial n}{\partial x} \pm \mu_\perp^\pm n E\right)
\end{aligned}$$

where ions and electrons are denoted by pluses and minuses, Ω is again the Hall parameter and the formalism is cast in a different axes convention. We get from Simon's coordinate system to ours in Fig. (4) by applying the transformations $x \to x$, $y \to z$ and $z \to -y$. The neglect of the temperature gradient in the above equations (cf Eq. (2)) greatly simplifies the problem as an energy equation is not needed. By using the flux conservation equation in its unsteady form

$$\frac{\partial n}{\partial t} + \boldsymbol{\nabla} \cdot \boldsymbol{\Gamma}_\pm = 0 \qquad (32)$$

one obtains a closed system of governing equations in $\tilde{n}$ and $\tilde{V}$, where $\tilde{V}$ is the oscillating electrostatic field. After linearizing with small perturbations the equations can be reduced to two sets of coupled differential equations in the unknown $\tilde{n}$ and $\tilde{V}$. Simon

uses the method of Kadmotsev-Nedospasov which requires trial solutions. The interested reader is referred to Simon's paper[31] for a discussion of the solution method and the boundary conditions. Having shown the governing equations, we now quote the resulting dispersion relation which, after straightforward manipulation and the neglect of non-flute modes (i.e. set $k_z = 0$), gives the following frequency and growth rate expressions:

$$\omega_r = \frac{\Psi k_y \dfrac{dn_0}{dx} \left[\Omega_i \mu_{\perp i} - \Omega_e \mu_{\perp e}\right] - \bar{n_0} \left(Y_i - Y_e\right) k_y \Theta}{\bar{n_0}^2 \left(Y_i + Y_e\right)^2 + k_y^2 \left(\dfrac{dn_0}{dx}\right)^2 \left[\Omega_i \mu_{\perp i} - \Omega_e \mu_{\perp e}\right]} \tag{33}$$

$$\gamma = \frac{\Psi \bar{n_0} \left(Y_i + Y_e\right)^2 + k_y^2 \Theta \dfrac{dn_0}{dx} \left[\Omega_i \mu_{\perp i} - \Omega_e \mu_{\perp e}\right]}{\bar{n_0}^2 \left(Y_i + Y_e\right)^2 + k_y^2 \left(\dfrac{dn_0}{dx}\right)^2 \left[\Omega_i \mu_{\perp i} - \Omega_e \mu_{\perp e}\right]} \tag{34}$$

with

$$\Psi = -\bar{n_0} \left(Y_e X_i + Y_i X_e\right), \tag{35}$$

$$X_s \equiv \Lambda^2 D_{\perp s} \tag{36}$$

$$Y_s \equiv \Lambda^2 \mu_{\perp s} \tag{37}$$

$$\Lambda^2 \equiv k_y^2 + \left(\frac{\pi}{l}\right)^2 \tag{38}$$

$$\Theta \equiv -\bar{E}_{0x} \bar{n}_0 \left[\Omega_i \mu_{\perp i} Y_e - \Omega_e \mu_{\perp e} Y_i\right] \tag{39}$$

$$+ \frac{dn_0}{dx} \left[\Omega_e \mu_{\perp e} X_i - \Omega_i \mu_{\perp i} X_e\right. \tag{40}$$

$$\left. + \frac{1}{2} \mu_{\perp i} \mu_{\perp e} \left(\Omega_i + \Omega_e\right) \frac{d\bar{E}_0}{dx}\right] \tag{41}$$

where we have used l, the finite spatial extent of the plasma in the x-direction. A quantity f that is under the bar must be evaluated using the following integral

$$\bar{f} = \frac{2}{l} \int_0^l f(x) \left(\frac{\pi x}{l}\right) dx \tag{42}$$

which results from the application of the boundary conditions as discussed by Simon.

We can now apply the above equations to our test case and use the numerator of Eq. (34) to find unstable roots ($\gamma > 0$).

The frequencies of the unstable oscillations (for a case of $l = 20$ mm, and the first purely azimuthal mode) are shown in Fig. (25) only for regions of instability. We note that according to the above formulation and calculations, azimuthal oscillations in the range of few tens of MHz can be excited. It seems to be quite a different mode from the high frequency azimuthal mode discovered by Esipchuck and Tilinin[21] since not only the frequencies are higher for our case but the mode is even excited in regions where $\partial B_r / \partial x > 0$.

4 Concluding Remarks

We have considered oscillations in the CDT over five frequency bands ranging from very low frequency up to tens of MHz. We used contours of various plasma parameters measured inside the accelerating channel of an SPT as the starting point of our investigation and calculated the magnitude and spatial distribution of various associated natural and collision frequencies, characteristic lengths and velocities. This extensive plasma characterization was then used to study the various bands of oscillations that are naturally excited in such thrusters.

The complex nature of the oscillations, which are excited by drifts and gradients of density and magnetic field, was revealed by evaluating various dispersion relations for our numerical case study. Much of the calculated characteristics had more than qualitative agreement with reported observations. We graphically illustrated the nature, character and spatial dependencies, of various modes including: low frequency azimuthal drift waves which formin a rotating spoke, axially propagating "transit-time" oscillations, high frequency azimuthal drift waves, ionization instability-type waves, and wave emission peculiar to weakly ionized plasma in crossed electric and magnetic fields.

This composite picture, the tools we used to bring it about, and the insight it may have engendered, should prove useful in our future attempts to develop a *predictive* model of the oscillations in such devices.

Acknowledgments I am thankful to Dr. Vladimir Kim, Dr. Slava Zhurin and Mr. Thomas Randolph for many helpful comments and fruitful discussions.

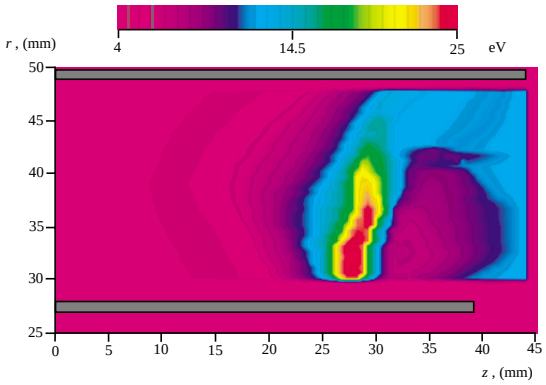

Figure 8: Electron temperature from the measurements of ref. [1]. (Average between x_1=2.5 cm and x_2=4 cm is 12.8 eV).

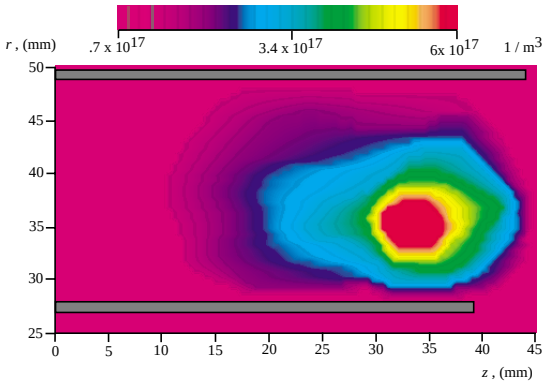

Figure 9: Charged species density from the measurements of ref. [1]. (Average between x_1 and x_2 is 3.3×10^{17} m^{-3}).

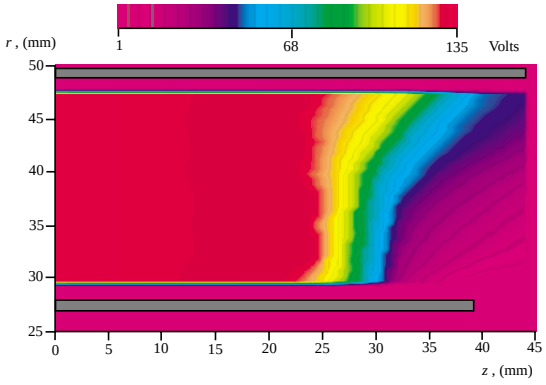

Figure 10: Floating potential from the measurements of ref. [1]. (Average between x_1 and x_2 is 73 V).

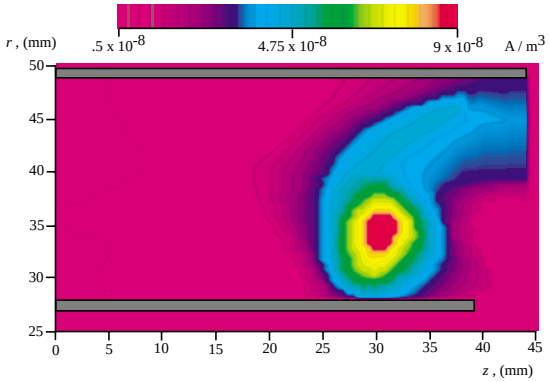

Figure 11: Charge production rate from the measurements of ref. [1]. (Average between x_1 and x_2 is 3.3×10^4 A/m^3).

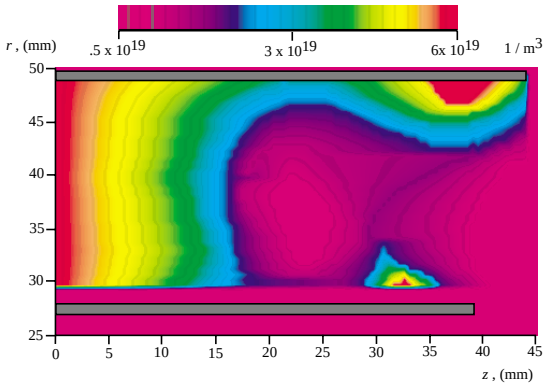

Figure 12: Neutral xenon density from the measurements of ref. [2]. (Average between x_1 and x_2 is 2×10^{19} m^{-3}).

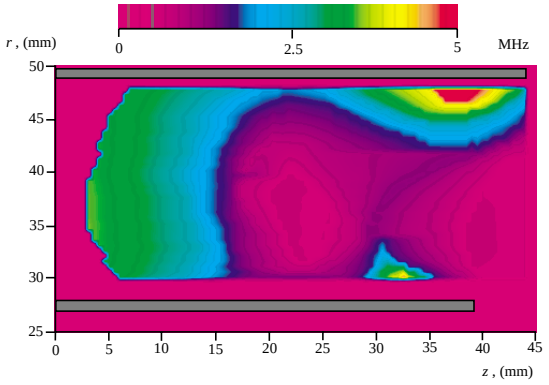

Figure 13: Total electron-neutral collision frequency. (Average between x_1 and x_2 is 1.53 MHz).

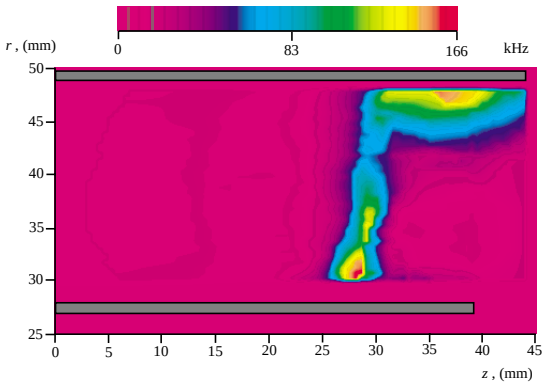

Figure 14: Ionization frequency. (Average between x_1 and x_2 is 35.3 kHz).

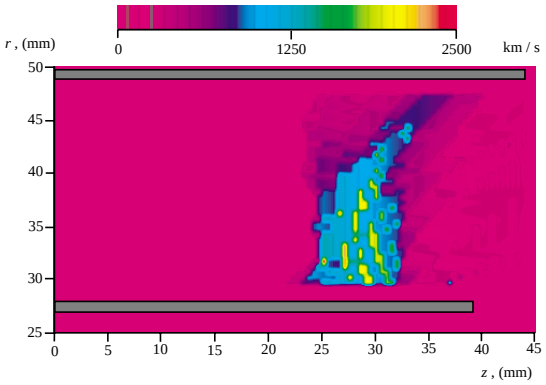

Figure 17: Electron azimuthal drift velocity. (Average between x_1 and x_2 is 690 km/s).

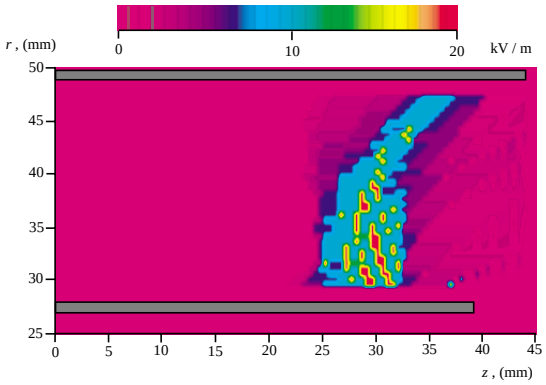

Figure 15: Axial electric field. (Average between x_1 and x_2 is 6.6 kV/m).

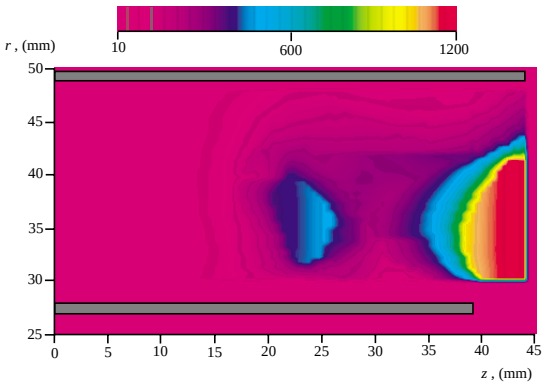

Figure 18: Electron Hall parameter. (Average between x_1 and x_2 is 286).

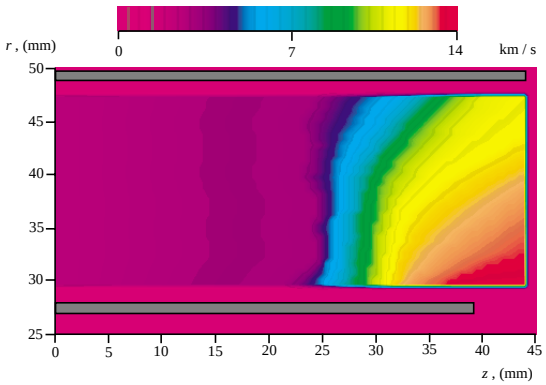

Figure 16: Ion velocity. (Average between x_1 and x_2 is 9.3 km/s).

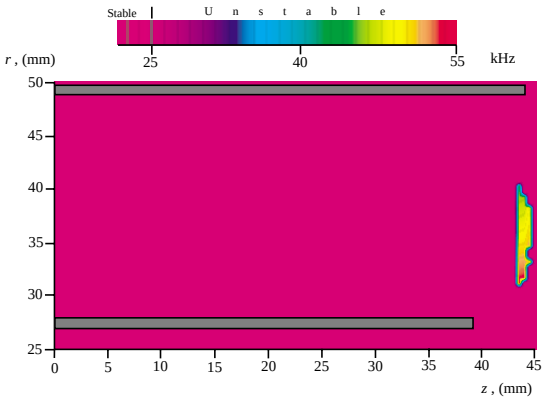

Figure 19: Frequency of unstable waves according to Eq. (18) for the first mode ($k = 1/r$) with largely azimuthal propagation ($k_y = 10\ k_x$). Purple=stable.

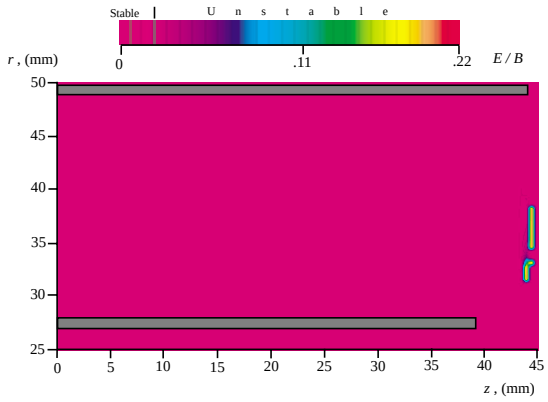

Figure 20: Phase velocity according to Eq. (18) for $(k = 1/r)$ with $(k_y = 10\ k_x)$. The phase velocity is normalized with the E_x/B_r. Purple=stable.

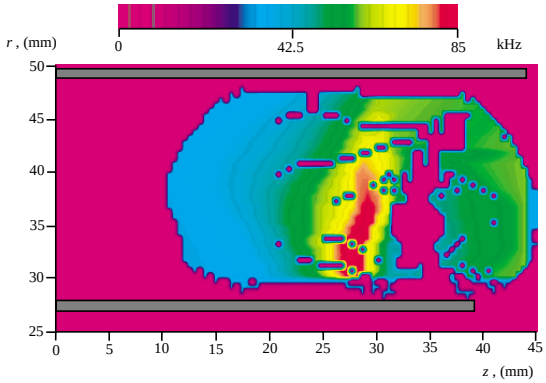

Figure 21: Minimum frequency of density-gradient-driven oscillations whose wavelengths are contained inside the channel. Purple=stable.

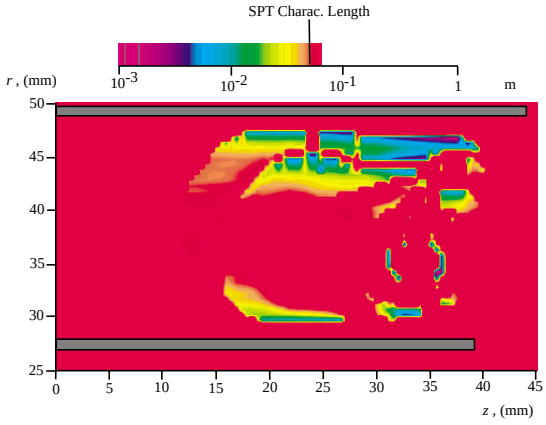

Figure 22: Minimum wavelengths of density-gradient-driven oscillations contained inside the channel.

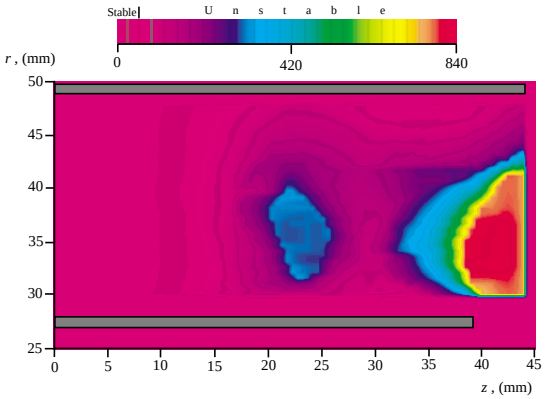

Figure 23: Criterion for the ionization instability according to Eq. (26). Purple denotes stability.

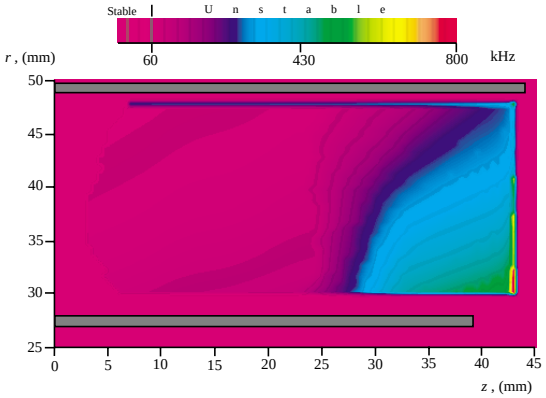

Figure 24: Frequency of unstable waves according to Eq. (18) and the condition in Eq. (29) for "transient-time" oscillations with largely axial propagation $(k_x = 10\ k_y)$. Purple=stable.

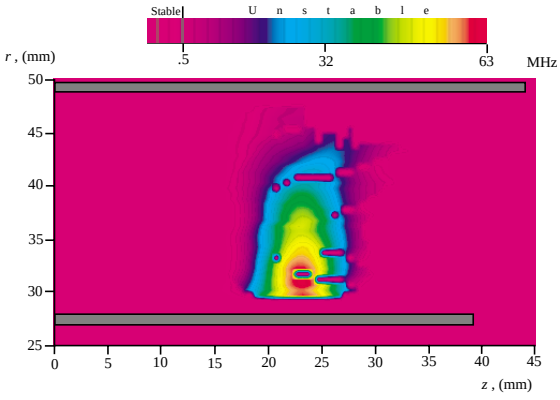

Figure 25: Frequency of unstable high frequency waves with azimuthal propagation. Purple=stable.

References

[1] A.M. Bishaev and V. Kim. Local plasma properties in a Hall-current accelerator with an extended acceleration zone. *Soviet Physics, Technical Physics*, 23(9):1055–1057, 1978.

[2] A.M. Bishaev, V.M. Gavryushin, A.I. Burgova, V. Kim, and V.K. Kharchvnikov. The experimental investigations of physical processes and characteritics of stationary plasma thrusters with closed drift of electrons. In 1^{st} *Russian-German Conference on Electric Propulsion Engines and their Tecnical Applications*, Giessen, Germany, 1992. RGC-EP 92-06.

[3] G.S. James and R. S. Lowder. Anomalous electron diffusion and ion accleration in a low-density plasma. *The Physics of Fluids*, 9(6):1115–1123, 1966.

[4] S.D. Grishin and L.V. Leskov. *Electrical Rocket Engines for Space Vehicles (Machine Translation from the Russian)*. Foreign Technology Division, WPAFB, Ohio, 89.

[5] H.R. Kaufmann. Technology of closed-drift thrsuters. *AIAA Journal*, 23(1):78, 1985.

[6] Artsimovich et.al. Development of a steady plasma engine (SPE) and its use on Meteor arificial satellite. *Kosmicheskie Issledovaniya*, 2(3):451–468, 1974.

[7] G.A. Popov and Y. A. Ryzhov. Electric propulsion in Russia and its practical applications. *Z. Fluwiss. Weltraumforsch*, 17:161–169, 1993.

[8] A.I. Morozov, Y. Epsinchuck, A.M. Kapulkin, V.A. Nevroskii, and V.A. Smirnov. Effect of the magnetic field on a closed-drift accelerator. *Soviet Physics, Technical Physics*, 17(2):482–487, 1972.

[9] J. Sankovic, J. Hamley, and T. Haag. Performance evaluation of the russian SPT-100 thrsuter at NASA-LeRC. In 23*rd International Electric Propulsion Conference*, Seattle, WA, USA, 1993. IEPC-93-094.

[10] J.R. Brophy, J.W. Barnett, J.M. Sankovic, and D.A. Barnhart. Performance of the stationary plsama thruster: SPT-100. In 28^{th} *Joint Propulsion Conference*, Nashville, TN, USA, 1992. AIAA-92-3155.

[11] R.M. Myers and D.H. Manzella. Stationary plasma thruster plume characteristics. In 23*rd International Electric Propulsion Conference*, Seattle, WA, USA, 1993. IEPC-93-096.

[12] L.H. Caveny, F.M. Curran, and J.R. Brophy. Russian electric propulsion evaluated for use on American small satellites. In 2^{nd} *German-Russian Electric Propulsion Conference*, Moscow, Russia, 1993. RGC-EP-93.

[13] Absalamov et. al. Measurement of plasma parameters in the SPT-100 plume and its effects on spacecraft components. In 28^{th} *Joint Propulsion Conference*, Nashville, TN, USA, 1992. AIAA-92-3156.

[14] V.I. Brukhty and K.P. Kiryashev. Electromagnetic interference of stationary plasma thruster. In 23*rd International Electric Propulsion Conference*, Seattle, WA, USA, 1993. IEPC-93-147.

[15] B.A. Arkhipov, R.Y. Gnizdor, N.A. Maslennikov, and A.I. Morozov. Anomalous erosion of an insulator under the action of a stream of plasma. *Soviet Journal of Plasma Physics*, 18(9):641–643, 1992.

[16] A.I. Morozov. Stationary plasma thruster (SPT) development steps and future perspectives. In 23^{rd} *International Electric Propulsion Conference*, Seattle, WA, USA, 1993. IEPC-93-101.

[17] D. Valentian and A. Burgova andA.I. Morozov. Development status of the SPT MK II thruster. In 23^{rd} *International Electric Propulsion Conference*, Seattle, WA, USA, 1993. IEPC-93-223.

[18] J. Hamley, G. Hill, and J. Sankovic. Power electronics development for the SPT-100 thruster. In 23^{rd} *International Electric Propulsion Conference*, Seattle, WA, USA, 1993. IEPC-93-044.

[19] A. Brown. *Basic Data of Plasma Physics*. McGraw-Hill Book Company, New York, 1959.

[20] Y.B. Esipchuck, A.I. Morozov, G.N. Tilinin, and A.V. Trofimov. Plasma oscillations in closed-drift accelerators with an extended acceleration zone. *Soviet Physics, Technical Physics*, 18(7):928–932, 1974.

[21] Y.B. Esipchuck and G.N. Tilinin. Drift instability in a Hall-current plasma accelerator. *Soviet Physics, Technical Physics*, 21(4):417–423, 1976.

[22] G.N. Tilinin. High-frequency plasma waves in a Hall accelerator with an extended acceleration zone. *Soviet Physics, Technical Physics*, 22(8):974–978, 1977.

[23] V. Kim, V. Kozlov, A. Sorokin, A. Isakov, and S. Kaminsky. For stages of work #1a-1d of extended contract # ks-2774560 between RIAME and SSL. Technical Report Work #1A-1D, RIAME, MAI, Moscow, Russia, 1993.

[24] V. Zhurin, J. Kahn, H. Kaufman, K. Kozubsky, and M. Day. Dynamic characteritics of closed drift thrusters. In 23^{rd} *International Electric Propulsion Conference*, Seattle, WA, USA, 1993. IEPC-93-095.

[25] A.M. Fridman. On the phenomena of the critical magnetic field and anomalous diffusion in weakly ionized plasma. *Soviet Physics, Doklady*, 9(1):75–77, 1964.

[26] M. Popovic and H. Melchior. Drift waves in a weakly ionized plasma. *Plasma Physics*, 10:495–498, 1968.

[27] A.B. Mikhailovskii. *Theory of Plasma Instabilities, Vol.2*. Consultants Bureau, New York, 1974.

[28] B.M. Smirnov. *Phyics of Weakly Ionized Gases*. Mir Publishers, Moscow, 1981.

[29] V. Zhurin, 1994. Front Range Research, Personal communication.

[30] G.G. Shishkin and V.F. Gerasimov. Plasma instabilities in acclerators with closed electron drift. *Soviet Physics, Technical Physics*, 20(9):1171–1174, 1976.

[31] A. Simon. Instability of a partially ionized plasma in crossed electric and magnetic fields. *Physics of Fluids*, 6(3):382–388, 1963.